

1 **Original Article**

2

3

4

MRI Cross Sectional Atlas of Normal Canine Cervical Musculoskeletal Structure

5

6

7

M. Alizadeh ^{a, *}, C. Zindl ^{b, **}, M.J. Allen ^b, G.G. Knapik ^a, N. Fitzpatrick ^c, W.S. Marras ^a

8

9

^a *Spine research Institute, The Ohio State University, 520 Baker Systems, 1971 Neil Avenue., Columbus, Ohio 43210 USA*

10

11

^b *Surgical Discovery Center, Department of Veterinary Medicine, University of Cambridge, Madingley Road, Cambridge, CB3 0ES, UK*

12

13

^c *Fitzpatrick Referrals, Eashing, Surrey GU7 2QQ, UK*

14

15

16

17

18

19

20

* Corresponding author. Tel.:+16787722108

21

22

E-mail address: alizadeh.3@osu.edu (Name: Mina Alizadeh).

23

Full postal address: The Ohio State University, Spine Research Institute, 1971 Neil Avenue

24

Room 520, Columbus, OH, USA. 43210.

25

26

*** Equally contributed to the work*

26

27 **Abstract**

28 Although magnetic resonance imaging (MRI) has been increasingly used as a
29 diagnostic tool for cervical spine injuries in canines, a comprehensive normal MRI anatomy
30 of the canine cervical spine muscles is lacking. Therefore, the purpose of this study was to
31 build a magnetic resonance imaging atlas of the normal cross sectional anatomy of the
32 muscles of the canine cervical spine. MRI scans were performed on a canine cadaver using a
33 combination of T1 and T2-weighted images in the transverse, sagittal and dorsal planes
34 acquired at a slice thickness of 1 mm. Muscle contours were traced manually in each slice,
35 using local osseous structures as reference points for muscle identification. Twenty-two
36 muscles were traced in 401 slices in the cervical region. A three dimensional surface model of
37 all the contoured muscles was created to illustrate the complex geometrical arrangement of
38 canine neck muscles. The cross-sectional area of the muscles was measured at the mid-level
39 of each vertebra. The accuracy of the location of the mapped muscles was verified by
40 comparing the sagittal view of the 3D model of muscles with still photographs obtained from
41 anatomic canine cadaver dissection. We believe this information will provide a unique and
42 valuable resource for veterinary researchers, clinicians and surgeons who wish to evaluate
43 MRI images of the cervical spine. It will also serve as the foundation for ongoing work to
44 develop a computational model of the canine cervical spine in which anatomical information
45 is combined with electromyographic, kinematic and kinetic data.

46

47

48

49 *Keywords:* dog; neck; cross sectional anatomy; magnetic resonance imaging

50

51 **1. Introduction**

52

53 Biomechanical cervical spine models have been used extensively to evaluate
54 feasibility and potential side effects of surgical procedures and instrumentation as it is
55 currently not feasible to directly measure spinal loading in-vivo (Jaeger et al., 2011).
56 Theoretical and numerical biomechanical models of the human cervical spine have been
57 developed over the last three decades to investigate kinetics and kinematics of the neck
58 (Dugailly et al., 2011). However, these models have not been translated to the canine cervical
59 spine in spite of the high incidence of spinal disorders and injuries (Jeffery et al., 2013).
60 Successful development and implementation of these models in canine spinal studies would
61 require accurate anatomical data of the underlying soft tissues and bone (Sharir et al., 2006).
62 Among the many components which should be incorporated into a model, muscles play a
63 vital role in stability, loading and locomotion as they exert the majority of the required
64 moments to maintain equilibrium in different postures and to perform various tasks
65 (Nussbaum et al., 1995; Vasavada et al., 1998). Studies have shown the substantial effect of
66 muscle forces on cervical spine kinematics and injury potential on the neck structure (Borst et
67 al., 2011). To this extent, comprehensive knowledge of canine muscle properties including
68 estimation of muscle forces and orientation has yet to be established.

69

70 The magnitude of the maximum muscle force generation potential in part depends on
71 the muscle morphometric parameters such as physiological cross-sectional area, muscle fiber
72 direction along the length of the muscle, and the muscle attachment site among many other
73 factors (Marras et al., 2001). Therefore, in order to develop an accurate canine specific
74 cervical model, the muscle cross-sectional area (CSA) needs to be directly measured and
75 incorporated.

76

77 These geometric properties are usually obtained from anatomic atlases, cadaveric
78 studies or medical images such as computed tomography (CT) and magnetic resonance
79 imaging (MRI). Regardless of technique, regional cross-sectional anatomy is of great
80 importance in identifying the muscle of interest and to determine its biomechanical properties
81 (Zotti et al., 2009). MRI has been used increasingly in dogs as a diagnostic technique for
82 musculoskeletal injuries, joint diseases and soft tissue tumors. It also had has become the
83 preferred imaging modality for investigating articular cartilage, meniscus and ligaments since
84 it provides excellent visualization of soft tissue (Soler et al., 2007; Van Caelenberg et al.,
85 2011; Zook et al., 1989). However a comprehensive search of the literature showed that
86 normal MRI cross-sectional anatomy of the canine neck muscles does not exist. George and
87 Smallwood 1992, had provided an atlas for head and neck using CT in the mesaticcephalic
88 dogs. Nevertheless, due to the inability of CT images to differentiate between muscles it is not
89 a comprehensive regional atlas for muscular structure of the canine neck. Hence, the primary
90 aim of this study was to 1) build a comprehensive atlas of cross-sectional anatomy of canine
91 cervical spine muscles using MRI datasets and 2) measure individual CSA of canine cervical
92 spine muscles at each cervical level. This would help to provide a suitable platform for the
93 potential development of a canine specific dynamic biomechanical model of the neck.

94 We believe that significant insights can be gained from MRI slice base representations.
95 This information will help researchers and clinicians to better evaluate MRI images and
96 enable them to precisely identify and visualize muscular structures of their interest. This
97 project will also be useful for surgeons during pre-operative planning helping identify
98 musculoskeletal structures in the canine neck area. Therefore the purpose of this study was
99 first to provide a cross-sectional anatomy atlas of the canine cervical spine muscles by tracing
100 them with different colors. Second, documenting major force producing neck muscles CSA

101

102 **2. Materials and methods**

103 *2.1 Specimen*

104

105 A skeletally mature male hound dog (26.0 kg body weight) that was euthanized for
106 reasons unrelated to this study served as the subject. The dog was healthy, with no evidence
107 of joint or spinal disease. It was housed in a single kennel in a room together with other dogs
108 and was fed a standard laboratory dog chow diet with water *ad libitum*. The experimental
109 procedures for this study were reviewed and approved by the local institutional animal care
110 and use committee (IACUC).

111

112 *2.2 MRI imaging*

113

114 T1 and T2 weighted MRI images were acquired on a 3T MRI scanner (Magnetom
115 Trio, Siemens Healthcare, Erlangen, Germany). Transverse slices of 1 mm thickness were
116 obtained from the skull level and extended caudally to the level of the second thoracic
117 vertebra. MRI examination was performed less than 1 hour after euthanasia to reduce
118 dehydration effects on muscles as much as possible. An MRI-compatible jig was designed to
119 aid in positioning the dog inside the MRI machine. The dog was positioned in ventral
120 recumbency with the thoracic limbs placed in an extended position next to the cervical area
121 and the neck kept in a fairly neutral posture by supporting the neck area with a pillow (Fig.1).

122

123

124 *2.3 Image analysis*

125 The files generated in DICOM format were retrieved and analyzed with Mimics®
126 software (Materialise NV Technologielaan 15, 3001 Leuven, Belgium). T1-weighted images
127 of all slices from the occiput to the first thoracic vertebra were analyzed. To begin with, bony

128 structures and muscles were differentiated with the thresholding and region growing
129 applications of the imaging program. Only left sided muscles were traced since it was
130 assumed that spinal musculature would be symmetric. Muscles were traced in each slice
131 based on the visible bony landmarks and the aid of literature about canine anatomy (Boyd et
132 al., 2001; Budras et al., 2007; Kumar, 2012; Miller and Christensen, 1964; Nickel et al.,
133 1992). Each muscle was assigned a separate mask to enhance visualization for outlining of
134 muscle borders and following CSA measurements (Fig 2-8). CSA of the traced muscles were
135 measured at the mid-level of each vertebra (Marras et al., 2001).

136

137 *2.4 Validation*

138 The relative locations of the different neck muscles were compared to photographic
139 images obtained during anatomic canine cadaver dissection. During dissection, the neck
140 muscles were visually identified and separated by removing connective tissues while
141 preserving each muscle's origin and insertion. Following the separation of the muscles,
142 photographs were obtained at different stages of the dissection to compare them with the
143 generated 3D models of the mapped muscles (Fig 9-11).

144

145 **3. Results**

146 *3.1 Canine cervical muscles mapped from MRI*

147 Twenty-two canine cervical spine muscles were traced and labeled on 441 transverse
148 MRI image slices (Fig 2-8). Only those muscles that play a role in movement of the neck and
149 partly in the head were considered and grouped as follows: 1. superficial and deep muscle
150 layers of the shoulder girdle; 2. long (superficial, medial, intermediate, deep layers) and short
151 muscles, representing extensors, rotators and neck lateral bending muscles; 3. neck flexors; 4.
152 movers of the head (Nickel et al., 1992; Schomacher and Falla, 2013).

153 From the superficial shoulder girdle muscle group, the M.trapezius cervicis,
154 M.omotransversarius, M.sternocephalicus, M.cleidomastoideus and M.cleidocervicalis as
155 parts of the M.brachiocephalicus; from the deep shoulder girdle muscle group, the
156 M.rhomboideus and M.serratus ventralis were included. The long neck muscles were
157 represented by the M.splenius as the superficial layer, the M.longissimus (capitis and
158 cervicis), M.longissimus thoracis and M.iliocostalis thoracis as part of the medium layer and
159 the M.spinalis et semispinalis cervicis, M.semispinalis capitis (biventer and complexus) and
160 M.multifidus cervicis as the deep layer. The short neck muscles were represented by the
161 M.intertransversarii cervicis only. On the ventral neck area, the M.longus colli and
162 M.scalenus were traced as the neck flexors. Included muscles that are considered movers of
163 the head were the M.longus capitis, M. rectus capitis dorsalis major, the M.obliquus capitis
164 (caudalis and cranialis) and the M.rectus capitis lateralis and M.rectus capitis ventralis. The
165 M.cleidobrachialis, M.interspinal cervicis, and the M.rectus capitis dorsalis minor were not
166 traced. A three dimensional (3D) model of all the identified and contoured muscles was
167 created to illustrate neck muscle location in 3D (Fig 8-9).

168

169 *3.2 Cross-sectional area of canine cervical muscles*

170 The CSA were measured in all 22 canine cervical muscles that were discriminated in MRI
171 images and results are shown in Table 1. Based on the length of the muscles, in this study,
172 they were grouped in three categories - long, medium and short muscles. The long muscles
173 are defined as extending either over the whole neck area, from C1-C2 into the thoracic area
174 This group includes the M.rhomboideus, M.splenius, M.semispinalis capitis (biventer and
175 complexus), and M.longissimus capitis. Or they are defined as extending over six vertebrae,
176 with additional segmental insertions / origins such as the M.longus capitis, M.longus colli,
177 M.intertransversarii cervicis. Medium muscles are defined as extending over either five

178 vertebrae such as the M.cleidocervicalis, M.sternocephalicus, M.cleidomastoideus,
179 M.omotransversarius, M.trapezius cervicis, M.spinalis et semispinalis cervicis, M.multifidus
180 cervicis and M.longissimus cervicis or over four vertebrae including the M.serratus ventralis
181 and M.scalenus. Short muscles are defined as those presented at only one level such as the
182 M.obliquus capitis cranialis, M.rectus capitis lateralis and M.rectus capitis ventralis or two
183 levels including M.obliquus capitis caudalis and M.rectus capitis dorsalis major.

184

185 **4. Discussion**

186 This study is part of an effort to develop a biologically-assisted musculoskeletal
187 canine cervical spine biomechanical model. Biomechanical models can be of great value in
188 identifying potential pathways for neck disorders. They represent a quantitative method to
189 evaluate mechanical effects of surgical techniques and interbody implants on spine. This
190 research provides fundamental information for the initial development of a canine cervical
191 spine model. However, in order to generalize the outcome of this study, more studies will be
192 necessary that involve more specimens. None the less, this study provides a platform for
193 future investigations. This study, for the first time, has implemented a well-developed precise
194 human biomechanical approach to quantify cervical spine muscle CSA (as opposed to
195 cadaveric studies which have several disadvantages).

196 In the present study we characterized the anatomical trajectory of the majority of the
197 canine cervical muscles with magnetic resonance imaging in a visual way to build an MRI
198 based cross-sectional atlas of the canine cervical spine muscles. Major force producing
199 muscles of the canine cervical spine were identified by measuring the cross-sectional area of
200 individual muscles.

201 MRI is a noninvasive cross-sectional imaging technique appropriate for diagnostic,
202 research and teaching purposes (Anastasi et al., 2007) with many advantages compared to

203 other medical imaging techniques (Alsafy, 2008). Soft tissues such as muscles are not readily
204 observed with other radiological modalities in a way that the borders between different
205 muscles can be distinguished. MRI provides excellent detail of clinically relevant anatomy
206 (Soler et al., 2007). Considering MRI spatial resolution, this imaging technique is more
207 sensitive in discriminating different soft tissues, detecting diseases and distinguishing normal
208 and abnormal structures and has been widely used in dogs in musculoskeletal imaging
209 (Adamiak et al., 2011; Agnello et al., 2008; De Bakker et al., 2014; Schaefer and Forrest,
210 2006) . However, accurate interpretation and identification of CT and MRI images require
211 comprehensive knowledge of the normal planimetric anatomy of the muscles in the region of
212 interest (Rivero et al., 2005).

213

214 This study denotes the musculoskeletal cross-sectional anatomy of the canine cervical
215 spine from the occiput to the first thoracic vertebra. Muscles on MRI images were identified
216 and classified with the help of several anatomy books describing the origin, trajectory and
217 insertion of the muscles in text and drawings (Miller and Christensen, 1964; Nickel et al.,
218 1992) together with photographs of cross-sectional reference cuts (Boyd et al., 2001; Kumar,
219 2012). The anatomic detail of some muscles showed slight discrepancy especially regarding
220 the photographs of the reference cuts, which was probably due to breed differences, as Boyd
221 et al (2001) used a Beagle for his study compared to the hound used in our study. This made
222 the differentiation and identification of muscles sometimes challenging.

223 Muscles with several portions were treated as a single muscle body regardless of their
224 different divisions as it was challenging to separate muscles into their distinguished bundles.
225 For instance, the M.intertransversarii cervicis anatomically consisting of the
226 M.intertransversarii dorsalis cervicis, the M.intertransversarii intermedii cervicis and the
227 M.intertransversarii ventralis cervicis, was considered as one single muscle body.

228 The ability to use all three imaging planes (sagittal, dorsal and transverse) at the same
229 time on one screen in the Mimics® software, made it easier to interactively distinguish and
230 mark the individual muscles. The 3D view substantially aided in the identification of muscles
231 in their complex geometrical arrangement as was described in an earlier study (Jaeger et al.,
232 2011).

233 The main purpose of this investigation was to map the major muscular actuators of
234 cervical motion. The emphasis was on defining the bulk of the muscle mass, since the origins
235 and insertions have been well established before; for this reason, the muscle bundles were not
236 separated into bundles and no attempt was made to map serrations. We mainly focused on
237 muscles that have major contributions to either moving or stabilizing the neck, regardless of
238 their role in shoulder or limb movements. Twenty-two muscles were identified and mapped,
239 the majority of those do play an active role in movement on the neck and head. We also
240 included some muscles of the shoulder girdle that participate in neck movement
241 (M.sternocephalicus, M.brachiocephalicus, M.rhomboideus and M.serratus ventralis). The
242 M.cleidobrachialis part of the M.brachiocephalicus was not mapped as its insertion on the
243 humerus was not in the field of view of the MR images – the same was true for the
244 M.pectoralis (superficialis and profundus). The M.platysma was not mapped because this
245 muscle was very difficult to identify on MR images due to its flat appearance and origin and
246 insertion points mainly emerging out of aponeuroses. We were not able to identify two of the
247 short neck muscles M.interspinal cervicis and the M.rectus capitis dorsalis minor with
248 confidence. These muscle bellies are small and either span a very short distance between
249 adjacent vertebrae or, in case of the M. rectus capitis dorsalis minor, become merged with the
250 M. rectus capitis dorsalis major. Furthermore, although muscles of the deep layer, such as the
251 M.intertransversarii cervicis were mapped, it was challenging and we were not able to trace
252 them precisely.

253 Several sequences are reported for use in MRI diagnostic imaging. The T1-weighted
254 images used in the present study to identify the individual muscles, have been reported to give
255 good anatomical detail to identify musculoskeletal structures (Agnello et al., 2008; Baeumlin
256 et al., 2010; Soler et al., 2007; Van Caelenberg et al., 2011). However, it was difficult to map
257 smaller muscles (M.interspinal cervicis and M. rectus capitis dorsalis minor). The muscle
258 size, unclear connective tissue borders between those muscles, and the inability to visually
259 separate muscles due to resolution factors of the 3T MRI machine are the factors that
260 contributed to prevent us from mapping those smaller muscles. The small voxel size of a 3T
261 MRI scanner gives a higher resolution. However, it leads to a much lower signal-to-noise
262 ratio which reduces the ability to identify small structures (Sunico et al., 2012). The same
263 study found that imaging the same specimen with a proton density sequence maximizes the
264 distinction of muscular borders compared to T1 or T2 sequences (Sunico et al., 2012).

265

266 In general the CSA measurements are not in agreement with the report by Sharir et al. (
267 2006). This conflict potentially might be due to several reasons, most probably as muscle
268 mass might be different between dogs of different breeds and also between individual
269 dogs. Muscle morphometric measurements were taken after dissection of the muscle in Sharir
270 et al (2006). Disturbing muscle connections with the surrounding connective tissue may affect
271 its anatomical properties such as its length and width, which might have influenced
272 measurements of the muscle cross section area. Different approaches were taken to present
273 muscle CSA, which increases the possibility of incompatibility between measurements. Sharir
274 et al., (2006) represented the physiological CSA of an individual muscle as a ratio of muscle
275 volume to its effective fascicle length while in the present study we measured actual CSA for
276 each muscle at different levels on MRI images. Therefore, in the study obtained by Sharir et
277 al., (2006), constant cross section throughout the length of the muscles was assumed.

278 Although this assumption might be valid for small muscles in the neck region, it is not an
279 appropriate representation for fan shaped muscles that have various attachments, as most of
280 the neck muscles present anatomically. These variations within the reported literature
281 highlight the need for quantitative assessments using up to date technological approaches.

282 The present study has several limitations. Only a single subject was evaluated, due to
283 the nature of this study being exploratory research. The ventral recumbency position of the
284 dog on the MRI table with the thoracic limbs positioned next to the cervical area with flexed
285 shoulder and elbow joints, might have resulted in altered muscle location and orientation in
286 comparison to a neutral standing position, with extended shoulder and elbow joints. By
287 positioning a pillow underneath the neck area, we tried to keep the neck posture as close as
288 possible to a posture in a standing position, however extended shoulder and elbow joints
289 could not be completely replicated. In spite of the excellent capability of MR images in
290 differentiating between muscles, it was still difficult to distinguish all muscles in the region of
291 interest, especially muscles of the deep layer. Therefore, we primarily aimed to identify
292 muscles in the superficial and medium layer of the neck region, as they are the main actuators
293 in stabilizing and moving the neck. With concurrent computed tomography imaging and
294 evaluation of photographic images of cross-sectional frozen cuts of the same individual, it
295 might have been possible to develop more accurate information to identify the muscles of the
296 deep layer on MR images, but this was beyond of the financial possibilities of this study.

297 While it is clear that there is likely to be significant breed-to-breed variation
298 particularly in muscle mass, we believe that the data presented in this study can be
299 implemented to develop a canine specific cervical biomechanical model as well as to be used
300 as a guide for future medical imaging investigations such as muscle bilateral symmetry
301 assumption.

302

303 **Conclusions**

304 The data from this work has allowed for the production of the first comprehensive
305 multi-segmental MRI atlas on the cross-sectional anatomy of the canine cervical spine
306 musculature. We anticipate that the 2D and 3D images from this work will be useful to
307 clinicians and researchers working with the canine cervical spine. They will also serve as the
308 foundation of a more expansive project to combine anatomical and EMG data to produce a
309 computational biomechanical model of the canine cervical spine that can be used to study the
310 impact of both pathology and surgical treatment on spinal kinetics and kinematics.

311

312 **Conflict of interest statement**

313 None declared.

314

315 **Acknowledgements**

316 This work was supported in part by Fitzpatrick Referrals Ltd., through the One Health/One
317 Medicine Fellowship at The Ohio State University.

318

319 **References**

- 320 Adamiak, Z., Jaskólska, M., Matyjasik, H., Pomianowski, A., Kwiatkowska, M., 2011.
 321 Magnetic resonance imaging of selected limb joints in dogs. *Pol. J. Vet. Sci.* 14, 501–
 322 505.
- 323 Agnello, K.A., Puchalski, S.M., Wisner, E.R., Schulz, K.S., Kapatkin, A.S., 2008. Effect of
 324 Positioning, Scan Plane, and Arthrography on Visibility of Periarticular Canine
 325 Shoulder Soft Tissue Structures on Magnetic Resonance Images. *Vet. Radiol.*
 326 *Ultrasound* 49, 529–539. doi:10.1111/j.1740-8261.2008.00429.x
- 327 Alsafy, M.A.M., 2008. Computed tomography and cross-sectional anatomy of the thorax of
 328 goat. *Small Rumin. Res.* 79, 158–166. doi:10.1016/j.smallrumres.2008.07.028
- 329 Anastasi, G., Bramanti, P., Di Bella, P., Favalaro, A., Trimarchi, F., Magaudda, L., Gaeta, M.,
 330 Scribano, E., Bruschetta, D., Milardi, D., 2007. Volume rendering based on magnetic
 331 resonance imaging: advances in understanding the three-dimensional anatomy of the
 332 human knee. *J. Anat.* 211, 399–406. doi:10.1111/j.1469-7580.2007.00770.x
- 333 Baeumlin, Y., De Rycke, L., Van Caelenberg, A., Van Bree, H., Gielen, I., 2010. Magnetic
 334 resonance imaging of the canine elbow: an anatomic study. *Vet. Surg.* VS 39, 566–
 335 573. doi:10.1111/j.1532-950X.2010.00690.x
- 336 Borst, J., Forbes, P.A., Happee, R., Veeger, D. (H. E.J.), 2011. Muscle parameters for
 337 musculoskeletal modelling of the human neck. *Clin. Biomech.* 26, 343–351.
 338 doi:10.1016/j.clinbiomech.2010.11.019
- 339 Boyd, J.S., Paterson, C., May, A.H., 2001. *Clinical anatomy of the dog & cat.* Harcourt
 340 Publishers Limited, Jamestown Road, London.
- 341 Budras, K.D., McCarthy, P.H., Fricke, W., Richter, R., Horowitz, A., Berg, R., 2007.
 342 *Anatomy of the Dog: An Illustrated Text, Fifth Edition.* Schluetersche, Germany.
- 343 De Bakker, E., Gielen, I., Kromhout, K., van Bree, H., Van Ryssen, B., 2014. Magnetic
 344 resonance imaging of primary and concomitant flexor enthesopathy in the canine
 345 elbow. *Vet. Radiol. Ultrasound Off. J. Am. Coll. Vet. Radiol. Int. Vet. Radiol. Assoc.*
 346 55, 56–62. doi:10.1111/vru.12090
- 347 Dugailly, P.-M., Sobczak, S., Moiseev, F., Sholukha, V., Salvia, P., Feipel, V., Rooze, M.,
 348 Van Sint Jan, S., 2011. Musculoskeletal modeling of the suboccipital spine:
 349 kinematics analysis, muscle lengths, and muscle moment arms during axial rotation
 350 and flexion extension. *Spine* 36, E413-422. doi:10.1097/BRS.0b013e3181dc844a
- 351 Evans, H.E., Lahunta, A. de, 2013. *Miller’s Anatomy of the Dog, 4th ed.* Saunders.
- 352 George, T.F., Smallwood, J.E., 1992. *Anatomic Atlas for Computed Tomography in the*
 353 *Mesaticephalic Dog: Head and Neck.* *Vet. Radiol. Ultrasound* 33, 217–240.
 354 doi:10.1111/j.1740-8261.1992.tb00136.x
- 355 Jaeger, R., Mauch, F., Markert, B., 2011. The muscle line of action in current models of the
 356 human cervical spine: a comparison with in vivo MRI data. *Comput. Methods*
 357 *Biomech. Biomed. Engin.* 15, 953–961. doi:10.1080/10255842.2011.567982
- 358 Jeffery, N. d., Levine, J. m., Olby, N. j., Stein, V. m., 2013. Intervertebral Disk Degeneration
 359 in Dogs: Consequences, Diagnosis, Treatment, and Future Directions. *J. Vet. Intern.*
 360 *Med.* 27, 1318–1333. doi:10.1111/jvim.12183
- 361 Kumar, M.S.A., 2012. *Clinically Oriented Anatomy of the Dog and Cat.* Linus Publications,
 362 Ronkonkoma, NY 11779.
- 363 Marras, W.S., Jorgensen, M.J., Granata, K.P., Wiand, B., 2001. Female and male trunk
 364 geometry: size and prediction of the spine loading trunk muscles derived from MRI.
 365 *Clin. Biomech.* Bristol Avon 16, 38–46.
- 366 Miller, M.E., Christensen, G. c., 1964. *Anatomy of the Dog, 4th ed.* Saunders company,
 367 philadelphia.

- 368 Nickel, R., Schummer, A., Seiferle, E., 1992. Lehrbuch der Anatomie der Haustiere, 6th ed.
369 Paul Parey, Berlin and Hamburg, Germany.
- 370 Nussbaum, M.A., Chaffin, D.B., Rechten, C.J., 1995. Muscle lines-of-action affect predicted
371 forces in optimization-based spine muscle modeling. *J. Biomech.* 28, 401–409.
- 372 Rivero, M.A., Ramírez, J.A., Vázquez, J.M., Gil, F., Ramírez, G., Arencibia, A., 2005.
373 Normal anatomical imaging of the thorax in three dogs: computed tomography and
374 macroscopic cross sections with vascular injection. *Anat. Histol. Embryol.* 34, 215–
375 219. doi:10.1111/j.1439-0264.2005.00596.x
- 376 Schaefer, S.L., Forrest, L.J., 2006. Magnetic Resonance Imaging of the Canine Shoulder: An
377 Anatomic Study. *Vet. Surg.* 35, 721–728. doi:10.1111/j.1532-950X.2006.00216.x
- 378 Schomacher, J., Falla, D., 2013. Function and structure of the deep cervical extensor muscles
379 in patients with neck pain. *Man. Ther.* 18, 360–366. doi:10.1016/j.math.2013.05.009
- 380 Sharir, A., Milgram, J., Shahar, R., 2006. Structural and functional anatomy of the neck
381 musculature of the dog (*Canis familiaris*). *J. Anat.* 208, 331–351. doi:10.1111/j.1469-
382 7580.2006.00533.x
- 383 Soler, M., Murciano, J., Latorre, R., Belda, E., Rodríguez, M.J., Agut, A., 2007.
384 Ultrasonographic, computed tomographic and magnetic resonance imaging anatomy
385 of the normal canine stifle joint. *Vet. J.* 174, 351–361. doi:10.1016/j.tvjl.2006.08.019
- 386 Sunico, S.K., Hamel, C., Styner, M., Robertson, I.D., Kornegay, J.N., Bettini, C., Parks, J.,
387 Wilber, K., Smallwood, J.E., Thrall, D.E., 2012. Two anatomic resources of canine
388 pelvic limb muscles based on CT and MRI. *Vet. Radiol. Ultrasound Off. J. Am. Coll.*
389 *Vet. Radiol. Int. Vet. Radiol. Assoc.* 53, 266–272. doi:10.1111/j.1740-
390 8261.2012.01926.x
- 391 Van Caelenberg, A.I., De Rycke, L.M., Hermans, K., Verhaert, L., van Bree, H.J., Gielen,
392 I.M., 2011. Low-field magnetic resonance imaging and cross-sectional anatomy of the
393 rabbit head. *Vet. J. Lond. Engl.* 1997 188, 83–91. doi:10.1016/j.tvjl.2010.02.020
- 394 Vasavada, A.N., Li, S., Delp, S.L., 1998. Influence of muscle morphometry and moment arms
395 on the moment-generating capacity of human neck muscles. *Spine* 23, 412–422.
- 396 Zook, B.C., Hitzelberg, R.A., Bradley, E.W., 1989. Cross-Sectional Anatomy of the Beagle
397 Thorax. *Vet. Radiol.* 30, 277–281. doi:10.1111/j.1740-8261.1989.tb01800.x
- 398 Zotti, A., Banzato, T., Cozzi, B., 2009. Cross-sectional anatomy of the rabbit neck and trunk:
399 comparison of computed tomography and cadaver anatomy. *Res. Vet. Sci.* 87, 171–
400 176. doi:10.1016/j.rvsc.2009.02.003

401
402
403
404

405

406

407

408

409

410

411 **Figure legends**

412 Fig.1. MRI of the occipital, cervical and cervico-thoracic area in the sagittal plane. Vertical
413 lines indicate the MRI slice corresponding to the presented images (Fig 2-8). The more cranial
414 slice represents section (a) and the more caudal slice represents section (b) of Figures 2-8.

415

416


417 Fig.2. T1-weighted MRI image at (C1). (a) Cranial C1. (b) Mid-vertebral C1. Muscles are
418 listed dorsal to ventral, left to right.

419  C1 and C2

420  M.cleidocervicalis


421  M.rhomboideus


422  M.splenius


423  M.cleidomastoideus


424  M.semispinalis capitis (Biventer)


425  M.semispinalis capitis (Complexus)


426  M.longissimus capitis


427  M.sternocephalicus

428  M. rectus capitis dorsalis major

429  M.obliquus capitis caudalis

430  M.obliquus capitis cranialis

431  M.rectus capitis lateralis


432  M. rectus capitis ventralis

433  M.longus capitis

434  M.longus colli

435


436 Fig.3. T1-weighted MRI image at (C2). (a) Cranial C2. (b) Mid-vertebral C2. Muscles are
437 listed dorsal to ventral, left to right.

438  Wing of Atlas (C1) and C2

439  M.cleidocervicalis


440  M.rhomboideus


441  M.splenius

442  M.cleidomastoideus


443  M.semispinalis capitis (Biventer)


444  M.semispinalis capitis (Complexus)


445  M.longissimus capitis


446  M.rectus capitis lateralis


447  M.omotransversarius

448  M.rectus capitis dorsalis major

449  M.obliquus capitis caudalis

450  M.sternocephalicus

451  M.rectus capitis ventralis

452  M.intertransversarii cervicis

453  M.longus capitis

454  M.longus colli

455

456



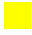

















457

458

459

460

461 Fig.4. T1-weighted MRI image at (C3). (a) Cranial C3. (b) Mid-vertebral C3. Muscles are
462 listed dorsal to ventral, left to right.

- 463  C3 and articular process of C4
- 464  M.trapezius cervicis
- 465  M.cleidocervicalis
- 466  M.rhomboideus
- 467  M.splenius
- 468  M.serratus ventralis
- 469  M.omotransversarius
- 470  M.cleidomastoideus
- 471  M.semispinalis capitis (Biventer)
- 472  M.semispinalis capitis (Complexus)
- 473  M.longissimus capitis
- 474  M.longissimus cervicis
- 475  M.intertransversarii cervicis
- 476  M.scalenus
- 477  M.longus capitis
- 478  M.sternocephalicus
- 479  Nuchal ligament
- 480  M.spinalis et semispinalis cervicis
- 481  M.multifidus cervicis
- 482  M.longus colli

483

484

485

486 Fig.5. T1-weighted MRI image at (C4). (a) Cranial C4. (b) Mid-vertebral C4. Muscles are
487 listed dorsal to ventral, left to right.

488 □ C4 (a, b) and tuberculum ventrale of transverse process of C3 (a)

489 ■ M.trapezius cervicis

490 ■ M.cleidocervicalis

491 ■ M.rhomboideus

492 ■ M.splenius

493 ■ M.serratus ventralis

494 ■ M.omotransversarius

495 ■ M.cleidomastoideus

496 ■ M.semispinalis capitis (Biventer)

497 ■ M.semispinalis capitis (Complexus)

498 ■ M.longissimus capitis

499 ■ M.longissimus cervicis

500 ■ M.intertransversarii cervicis

501 ■ M.scalenus

502 ■ M.longus capitis

503 ■ M.sternocephalicus

504 ■ Nuchal ligament

505 ■ M.spinalis et semispinalis cervicis





















506 ■ M.multifidus cervicis

507 ■ M.longus colli

508

509


510 Fig.6. T1-weighted MRI image at (C5). (a) Cranial C5. (b) Mid-vertebral C5. Muscles are
511 listed dorsal to ventral, Left to Right.


- 512  C4 articular process and C5
- 513  M.trapezius cervicis
- 514  M.rhomboideus
- 515  M.splenius
- 516  M.serratus ventralis
- 517  M.cleidocervicalis
- 518  M.omotransversarius
- 519  M.semispinalis capitis (Biventer)
- 520  M.semispinalis capitis (Complexus)
- 521  M.longissimus capitis
- 522  M.longissimus cervicis
- 523  M.intertransversarii cervicis
- 524  M.scalenus
- 525  M.longus capitis
- 526  M.cleidomastoideus
- 527  M.sternocephalicus
- 528  Nuchal ligament
- 529  M.spinalis et semispinalis cervicis
- 530  M.multifidus cervicis
- 531  M.longus colli

532


533

534 Fig.7. T1-weighted MRI image at (C6). (a) Cranial C6. (b) Mid-vertebral C6. Muscles are
535 listed dorsal to ventral, left to right.

536  C6


537  Articulatio humeri (a) and Scapula (b)

538  M.trapezius cervicis


539  M.omotransversarius


540  M.rhomboideus


541  M.splenius


542  M.serratus ventralis

543  M.semispinalis capitis (Biventer)


544  M.semispinalis capitis (Complexus)


545  M.longissimus capitis

546  M.longissimus cervicis


547  M.longissimus thoracis and M.illiocostalis thoracis

548  M.scalenus

549  Nuchal ligament


550  M.spinalis et semispinalis cervicis

551  M.multifidus cervicis

552  M.intertransversarii cervicis

553  M.longus capitis


554  M.longus colli

555  M.sternocephalicus


556

557

558 Fig.8. T1-weighted MRI image at Mid-vertebral level (C7). Muscles are listed dorsal to
559 ventral, left to right.


560  C7


561  Scapula

562  M.trapezius cervicis

563  M.rhomboideus


564  M.splenius


565  M.serratus ventralis


566  M.semispinalis capitis (Biventer)


567  M.semispinalis capitis (Complexus)


568  M.longissimus capitis


569  M.longissimus cervicis

570  M.longissimus thoracis and M.illiocostalis thoracis

571  M.intertransversarii cervicis

572  Nuchal ligament

573  M.spinalis et semispinalis cervicis

574  M.multifidus cervicis

575  M.longus colli

576

577

578

579

580

581

582 Fig.9. Sagittal left lateral view of the superficial shoulder girdle muscles (a) 3D image of
583 mapped muscles. (b) Photographic image of the anatomic canine cadaver dissection. 1 -
584 M.cleidocervicalis; 2 – M.trapezius cervicis; 3 –M. sternocephalicus.

585

586 Fig.10. Sagittal lateral view from the left of the superficial and deep shoulder girdle muscles
587 and the superficial long neck muscle (a) 3D image of mapped muscles. (b) Photographic
588 image of the anatomic canine cadaver dissection. 1- M.rhomboideus; 2 - M.splenius; 3 -
589 M.serratus ventralis; 4 - M.omotransversarius.

590

591

592

593

594

595

596

597

598

599

600

601

602

603

604

605

606